Dynamical properties of mutually delayed coupled semiconductor lasers

H. Erzgräber[a], D. Lenstra[a,d], B. Krauskopf[b,a], I. Fischer[c]

[a]Faculty of Science, Vrije Universiteit Amsterdam, De Boelelaan 1081 HV, Amsterdam, The Netherlands

[b]Department of Engineering Mathematics, University of Bristol, Bristol BS8 1TR, UK

[c]Institut für Angewandte Physik, Technische Universität Darmstadt, Schloßgartenstraße 7, D-64289 Darmstadt, Germany

[d]Research Institute COBRA, Technical University Eindhoven, The Netherlands

ABSTRACT

We theoretically investigate the dynamical properties of a system of two semiconductor lasers that are mutually coupled via their optical fields. An intrinsic feature of the coupling is its time delay which generically arises from the finite propagation time of the light form one laser to the other. In our system the coupling time is in the sub-ns range, which is of the same order of magnitude as the period of laser's internal relaxation oscillations. We model this system with Lang-Kobayashi-type rate equations where we account for the mutual coupling of the two lasers by a delay term. The resulting set of nonlinear delay differential equations is analyzed by using recently developed numerical continuation. We consider the case of two nearly identical lasers with symmetrical coupling conditions but different frequencies, and present an analysis of the coupled laser modes (CLMs) of the system.

Keywords: mutually coupled lasers, delay differential equations, numerical continuation

1. INTRODUCTION

Semiconductor lasers are known to be very sensitive to external optical perturbation, for example to external reflection of their own light or the influence of another laser. The case that we are concerned with here is that of two mutually coupled lasers. This case has received increasing interest recently, both experimentally as well as theoretically. In [1, 2] synchronization of two chaotic semiconductor lasers is reported. In [3] spontaneous symmetry breaking and a leader-laggard scenario is found and the effect of detuning is investigated. Theoretical investigations have been done in [4] for the instantaneous coupling limit, whereas in [5] the focus is on the long coupling time limit. In [6] a thermodynamic potential for two mutually coupled laser is derived and investigated. First experiments on mutually coupled lasers in the short coupling time regime are presented in [7], showing the influence of spectral detuninig. In [8] recent experiments are presented that show the importance of the coupling phase in good agreement with numerical results based on rate equations.

In this contribution we consider a system of two nearly identical semiconductor lasers. The lasers are coherently mutually coupled via their optical fields, that is, light from one laser is injected into the other laser and vice versa. We focus on a coupling time regime where the coupling time is of the same order of magnitude as the laser's internal relaxation oscillation, thus, it is not negligible and the full delay differential equations (DDEs) must be studied. To analyze the structure of the solutions, we use DDE-BIFTOOL, a recently developed numerical continuation software package for DDEs; see [9]. Supplied with an approximate starting solution, such as an equilibrium or a periodic orbit, DDE-BIFTOOL allows one to follow this solution in one free parameter, irrespective of its stability. Along such a branch of solutions stability information can be computed and bifurcations detected.

Further author information: (Send correspondence to H. Erzgräber)
E-mail: H.Erzgraber@few.vu.nl

We describe the mutually coupled laser system with a set of Lang-Kobayashi-type rate equations for the normalized complex slowly-varying envelope of the optical fields $E_{1,2}$ and the normalized inversions $N_{1,2}$; see [10]. The optical fields of the lasers are represented by $E_i(t)e^{i\Omega_0 t}$, where $\Omega_0 = \frac{1}{2}(\Omega_1+\Omega_2)$ and Ω_i is the optical frequency of laser i operated solitarily, that is, when it is not coupled to the other laser. Apart form their possibly different solitary optical frequencies the two lasers are considered to have identical parameters. The equations can be written as

$$\frac{dE_1}{dt} = (1+i\alpha)N_1(t)E_1(t) + \eta e^{-iC_p}E_2(t-\tau) - i\Delta E_1(t)\,, \tag{1}$$

$$\frac{dE_2}{dt} = (1+i\alpha)N_2(t)E_2(t) + \eta e^{-iC_p}E_1(t-\tau) + i\Delta E_2(t)\,, \tag{2}$$

$$T\frac{dN_1}{dt} = P - N_1(t) - (1+2N_1(t))|E_1(t)|^2\,, \tag{3}$$

$$T\frac{dN_2}{dt} = P - N_2(t) - (1+2N_2(t))|E_2(t)|^2\,. \tag{4}$$

A detailed derivation of these equations can be found in [2]. In these equations time t is measured in units of the photon lifetime. The mutual coupling is described by the second term on the right hand side of (1) and (2). An intrinsic feature of the coupling is the time delay τ, which is due to the finite propagation time of the light between the spatially separated lasers. A possible spectral detuning is taken into account by the last term of (1) and (2) where $\Delta = \frac{1}{2}(\Omega_2 - \Omega_1)$. An important parameter in this contributions is the coupling phase $C_p = \Omega_0\tau$, which we consider as an independent parameter. This is reasonable since tiny changes of τ or Ω_0 have only little effect on the other parameters. The remaining parameters are the linewidth enhancement factor α, the coupling strength η, the normalized carrier lifetime T and the pump parameter P. For all these parameters we adapt physically meaningful values namely, $\tau = 71$ $\alpha = 5.0$, $\eta = 0.025$, $T = 392.7$, and $P = 0.231$. In physical units these values correspond to a coupling time of 0.2 ns, a coupling strength of 8.9×10^9 s^{-1}, a carrier life time of 1.1×10^{-9} s, photon lifetime of 2.8×10^{-12} s and a pump current which is 1.5 times above the threshold pump current.

Equations (1)–(4) exhibit several symmetries which we discuss now. First, there is the S^1-symmetry $(E_1, E_2, N_1, N_2) \to (E_1e^{ib}, E_2e^{ib}, N_1, N_2)$, which is a typical feature of Lang-Kobayashi-type optical feedback, provided that no phase conjugation is involved [11]. Thus, any solution is invariant under any phase shift of both electric fields E_1 and E_2, which is a real phase-space symmetry as no parameters are involved. The S^1-symmetry motivates the ansatz (5)–(8) of the coupled laser modes (CLMs) of section 2 with a common frequency for both lasers. Second, there is the reflection symmetry $(E_1, E_2, N_1, N_2, \Delta) \to (E_2, E_1, N_2, N_1, -\Delta)$, involving an interchange of the lasers and a sign change of Δ. For zero detuning, that is for $\Delta = 0.0$, this implies an additional Z_2-symmetry of exchanging laser 1 with laser 2, without changing any parameter. This is already an indication of the pitchfork bifurcations (also called symmetry breaking bifurcation), which are indeed found in section 3. Third, there is a 2π-translational symmetry $(E_1, E_2, N_1, N_2, C_p) \to (E_1, E_2, N_1, N_2, C_p + 2\pi)$, involving the parameter C_p. Following a solution over a C_p interval of 2π contains all information, nevertheless it is often more practical to follow C_p over several periods of 2π. Finally, there is a π-translational symmetry $(E_1, E_2, N_1, N_2, C_p) \to (E_1, -E_2, N_1, N_2, C_p + \pi)$, which involves a change of C_p by π and a sign change in either E_1 or E_2. The π-translational symmetry gives a link between what we call in-phase CLMs and anti-phase CLMs; see section 2.

In the following section we will give a comprehensive overview over the basic solutions of the system and derive analytical expressions for the in-phase and anti-phase CLMs for zero detuning. In section 3 we perform numerical continuation for the zero detuning case, revealing the existence of another type of solutions, the variable-phase CLMs. In section 4 we discuss the CLMs for nonzero but fixed detuning. The CLMs are discussed in section 5 as a function of the detuning. Finally, we also compare the theoretical results with an experiment. We finish with conclusions and outlook.

2. COUPLED LASER MODES

Guided by physical intuition and taking into account the symmetries discussed in section 1 we try the ansatz:

$$E_1(t) = R_1^s e^{i\omega^s t}\,, \tag{5}$$

$$E_2(t) = R_2^s e^{i\omega^s t + i\sigma}\,, \tag{6}$$
$$N_1(t) = N_1^s\,, \tag{7}$$
$$N_2(t) = N_2^s\,. \tag{8}$$

where R_i^s, N_i^s, ω^s, and σ are time independent and real valued; additionally, the R_i^s are taken to be positive. We allow different steady state amplitudes R_i^s and different steady state inversions N_i^s. However, the lasers must have the same frequency ω^s in agreement with the S^1-symmetry, where ω^s describes the deviation between the solitary laser frequency and the frequency of the coupled laser system. Note that there may be some time-independent phase shift σ between the lasers. We call solutions (5)–(8) coupled laser modes (CLMs); physically, they are continuous wave solutions. Inserting this ansatz into (1)–(4) gives a set of six coupled nonlinear transcendental equations for the six unknowns:

$$0 = R_1^s N_1^s + \kappa R_2^s \cos(-C_p - \omega^s\tau + \sigma)\,, \tag{9}$$
$$(\omega^s + \Delta)R_1^s = \alpha R_1^s N_1^s + \kappa R_2^s \sin(-C_p - \omega^s\tau + \sigma)\,, \tag{10}$$
$$0 = R_2^s N_2^s + \kappa R_1^s \cos(-C_p - \omega^s\tau - \sigma)\,, \tag{11}$$
$$(\omega^s - \Delta)R_2^s = \alpha R_2^s N_2^s + \kappa R_1^s \sin(-C_p - \omega^s\tau - \sigma)\,, \tag{12}$$
$$0 = P - N_1^s - (1 + 2N_1^s)|R_1^s|^2\,, \tag{13}$$
$$0 = P - N_2^s - (1 + 2N_2^s)|R_2^s|^2\,. \tag{14}$$

We can use (9)–(12) and eliminate the unknown variables R_1, R_2, N_1, N_2. The result is a transcendental equation containing ω^s and σ, namely:

$$\begin{aligned}(\omega^s + \Delta)(\omega^s - \Delta) = {} & \kappa^2(\sin(C_p + \omega^s\tau + \sigma) + \alpha\cos(C_p + \omega^s\tau + \sigma)) \\ & \times(\sin(C_p + \omega^s\tau - \sigma) + \alpha\cos(C_p + \omega^s\tau - \sigma))\,.\end{aligned} \tag{15}$$

So far there is no comprehensive geometrical picture available for the general solutions of (9)–(14). However, for zero detuning we can derive some analytical expressions.

3. ZERO DETUNING

When one sets $\Delta = 0.0$ one can see immediately that $\sigma = 0$ and $\sigma = \pi$ gives a transcendental equation for ω^s similar to that for conventional optical feedback [12]:

$$\omega^s = \mp[\kappa(\sin(C_p + \omega^s\tau) + \alpha\cos(C_p + \omega^s\tau))]\,. \tag{16}$$

The minus sign gives the in-phase CLMs with $\sigma = 0$ and the plus sign gives the anti-phase CLMs with $\sigma = \pi$. For these CLMs $\sigma = const.$, that is, σ is independent of C_p. Thus, we also refer to them as constant-phase CLMs. For all constant-phase CLMs one finds that $N_1^s = N_2^s$ and $R_1^s = R_2^s$.

In Fig. 1(a) the inversion N is plotted as a function of the frequency ω^s. The filled circles in Fig. 1(a) mark the position of the in-phase CLMs for fixed $C_p = 0.0$, of which there are five. The filled squares in Fig. 1(a) mark the positions of the anti-phase CLMs for fixed $C_p = 0.0$, of which there are also five. We indicate the inversion of laser 1 by filled symbols and inversion of laser 2 by open symbols. Since $N_1 = N_2$, the open symbols can not be distinguished from the filled symbols. The ellipse on which these CLMs lie can be found by following the CLMs as C_p is changed over 2π. Note that the π-translational symmetry interchanges the circles with the squares in Fig. 1(a) and vice versa.

Now we look for more general solutions, where σ is some function of C_p, and $N_1^s \neq N_2^s$ and $R_1^s \neq R_2^s$, which we call variable-phase CLMs. For these type of CLMs, there is no comprehensive geometrical picture available yet. However, we can use the full set of equations (9)–(14) and apply Newton's method to find solutions. Five variable-phase CLMs are found for fixed $C_p = 0.0$. In Fig. 1(b) these CLMs are plotted in the (ω^s, N^s)-plane. The filled triangles mark the inversion of laser 1 and the open triangles mark the inversion of laser 2. There is a second set of symmetrically related variable-phase CLMs: applying the reflection symmetry to Fig. 1(b) interchanges the filled triangles with the open triangles. All variable-phase CLMs also lie on a closed curve that

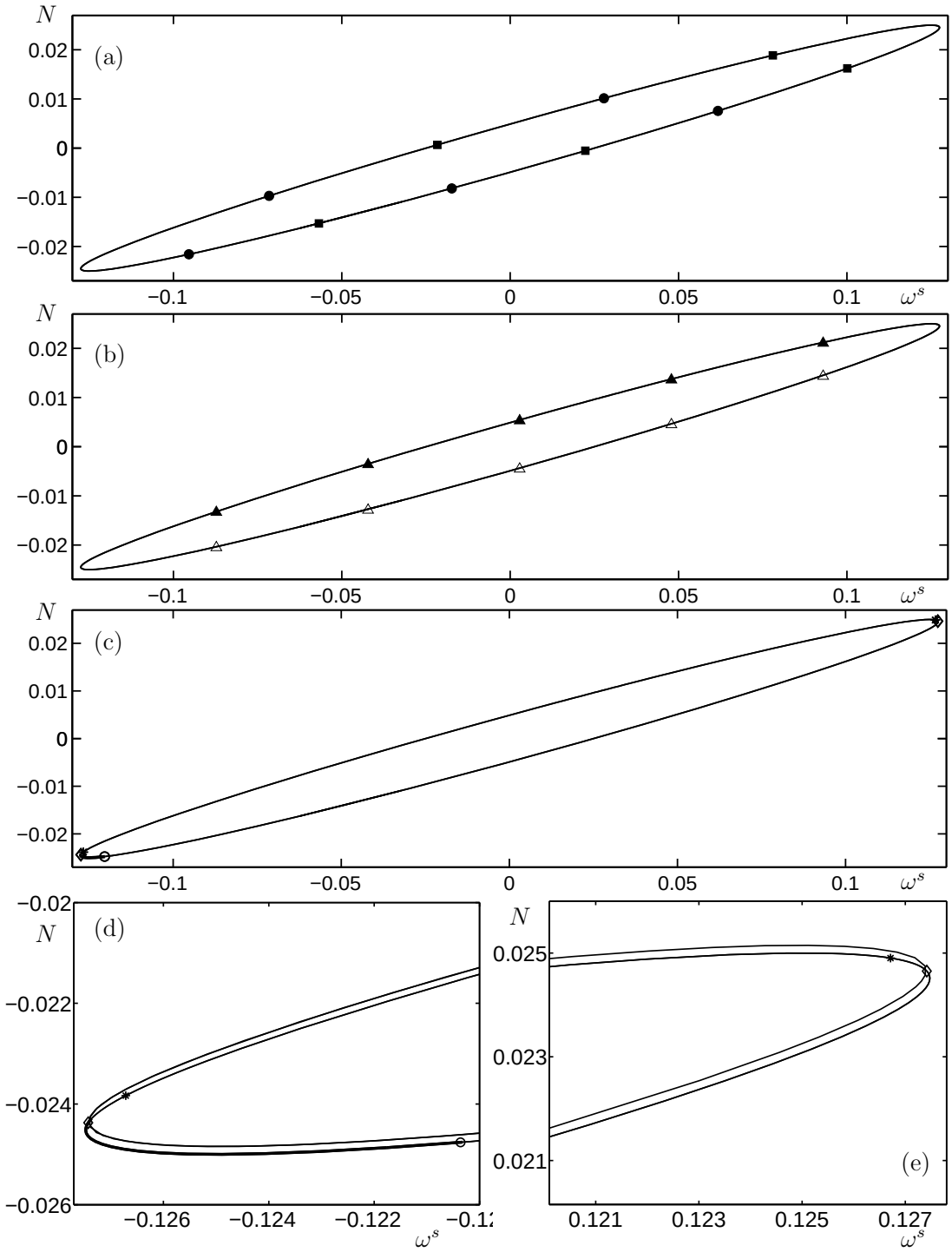

Figure 1. Ellipses of CLMs for zero detuning in the (ω^s, N)-plane, where C_p is varied. Panel (a) shows the constant-phase CLM ellipse with in-phase solutions (circles) and anti-phase solutions (squares) for $C_p = 0.0$. Filled symbols are for laser 1 and open symbols are for laser 1. Note that $N_1 = N_2$ for constant-phase CLMs. Panel (b) shows the variable-phase CLM ellipse with CLMs for $C_p = 0.0$ indicated by filled triangles for laser 1 and open triangles for laser 2. Panel (c) shows the constant-phase CLM ellipse; stars ($*$) mark saddle-node bifurcations, diamonds ($\diamond$) pitchfork bifurcations, and circles ($\circ$) Hopf bifurcations. Panels (d) and (e) show an enlarged view of the low-inversion region and the high-inversion region, respectively, emphasizing the difference between the constant-phase ellipses and the variable-phase ellipses.

also appears to be an ellipse. This ellipse can be found by varying C_p over 2π. At the scale of Fig. 1(b) the variable-phase ellipse cannot be distinguished from the constant-phase ellipse of Fig. 1(a). However, the two ellipses are indeed different as can be seen in Fig. 1(d) and Fig. 1(e).

So far we discussed the situation for a fixed value of C_p. When C_p is decreased continuously the CLMs in Fig. 1(a) move continuously from the low-inversion region towards the high-inversion region along the ellipse, indicated in the figure. The constant-phase CLMs are pairwise born in a saddle-node bifurcation in the low-inversion region, and destroyed pairwise in a saddle-node bifurcation in the high-inversion region. In Fig. 1(c) only the ellipse of Fig. 1(a) is plotted without CLMs for fixed C_p. The marks indicate points where the constant-phase CLMs undergo certain bifurcations while they move along the ellipse as C_p is varied. Saddle-node bifurcations are marked by stars ($*$), pitchfork bifurcations by diamonds ($\diamond$) and Hopf bifurcations by circles ($\circ$). The boldfaced part of the ellipse in the low-inversion region marks the region where stable CLMs can be found. For the chosen parameter values only one of the constant-phase CLM can be found in the stable region, that is, either one in-phase CLM or one anti-phase CLM. The stable part of the ellipse is bounded by a Hopf bifurcation on the right-hand side and a pitchfork bifurcation on the left-hand side. This pitchfork bifurcation gives rise to the variable-phase CLMs and marks the point where the constant-phase ellipse intersects the variable-phase ellipse. When an in-phase CLM crosses the pitchfork bifurcation in the low-inversion region two variable-phase CLMs are born, related to each other by the reflection symmetry. For decreasing C_p the variable-phase CLMs also move along their ellipse from the low-inversion region towards the high-inversion region. The ellipse is already indicated in Fig. 1(b). The variable-phase CLMs are destroyed in the pitchfork bifurcation in the high-inversion region. However, during this journey the variable-phase CLM accumulates an extra phase of π. Thus, the variable-phase CLMs provide a connection between the in-phase and the anti-phase CLMs and vice versa. The same happens to variable-phase CLMs that are born in a pitchfork bifurcation of an anti-phase CLM. Therefore, applying the π-translational symmetry does not change Fig. 1(b), because we do not distinguish between variable-phase CLMs that are born in a pitchfork bifurcation of either an in-phase CLM or an anti-phase CLM.

4. NONZERO DETUNING

First we present a global picture of the CLMs for nonzero detuning as a function of C_p. We want to know along which curve the CLMs move for $\Delta \neq 0$ in the (ω^s, N^s)-plane when C_p is changed. For convenience, in Fig. 2(a) and Fig. 2(b) we plotted the rescaled inversions $N^* = N - 0.19\omega^s$ of laser 1 and laser 2, respectively. This shearing transformation plots N relative to the long axis of the zero detuning ellipses in Fig. 1. In the following we choose laser 2 being positively detuned with respect to laser 1. Thus, we can refer to laser 1 as the red laser and to laser 2 as the blue laser. In the (N_1^*, ω^s)-plane of Fig. 2(a) a horseshoe can be seen, that opens to the right-hand side. Whereas, in the (N_2^*, ω^s)-plane of Fig. 2(b) a horseshoe can be seen, that open to the left-hand side. Both horseshoes are obtained by following one CLM under variation of C_p and keeping all other parameters fixed. Again the CLMs undergo certain bifurcations when C_p is changed. Four saddle-node bifurcations ($*$) can be found. They are labeled by the letters 'a,b,c,d'. Two of them, 'a' and 'd', are remainders of the pitchfork bifurcation for zero detuning. The other two, 'b' and 'c', were already present for zero detuning. Several Hopf bifurcations are found. We only plot the Hopf bifurcation ($\circ$) which bounds the stable region. Again for a fixed value of C_p a fixed number of CLMs can be found and only one CLM lies in the stable region at the same time.

Furthermore, we present what happens to σ when moving along the CLM branch, and plot in Fig. 2(c) σ as a function of ω^s. A closed curve can be seen, where we define a direction along this curve by arrows; each branch is marked by a different style of arrow. One can see that there are two branches of almost constant in-phase or anti-phase CLMs. They are connected by two branches of decreasing and increasing variable-phase CLMs.

Let us first consider the branch between the saddle-node bifurcations 'a' and 'b' of decreasing σ indicated by arrow ($\rightarrow$). In Fig. 2(a) this is the upper branch of the upper half of the blue laser's horseshoe. Correspondingly, it is the upper branch of the lower half of the red laser's horseshoe in Fig. 2(b). The next branch between saddle-node bifurcations 'b' and 'c' ($\Longleftarrow$) is a branch of almost constant $\sigma \simeq 0$. It corresponds to the lower branch of the upper half of the blue horseshoe and the lower branch of the upper half of the red horseshoe. The branch between saddle-node bifurcations 'c' and 'd' ($\longrightarrow$) is a branch of increasing σ. It corresponds to the upper branch of the lower half of the blue horseshoe and the upper branch of the upper half of the red horseshoe. Finally, the branch between saddle-node bifurcations 'd' and 'a' ($\Leftarrow$) is a branch of almost constant $\sigma \simeq \pi$. It

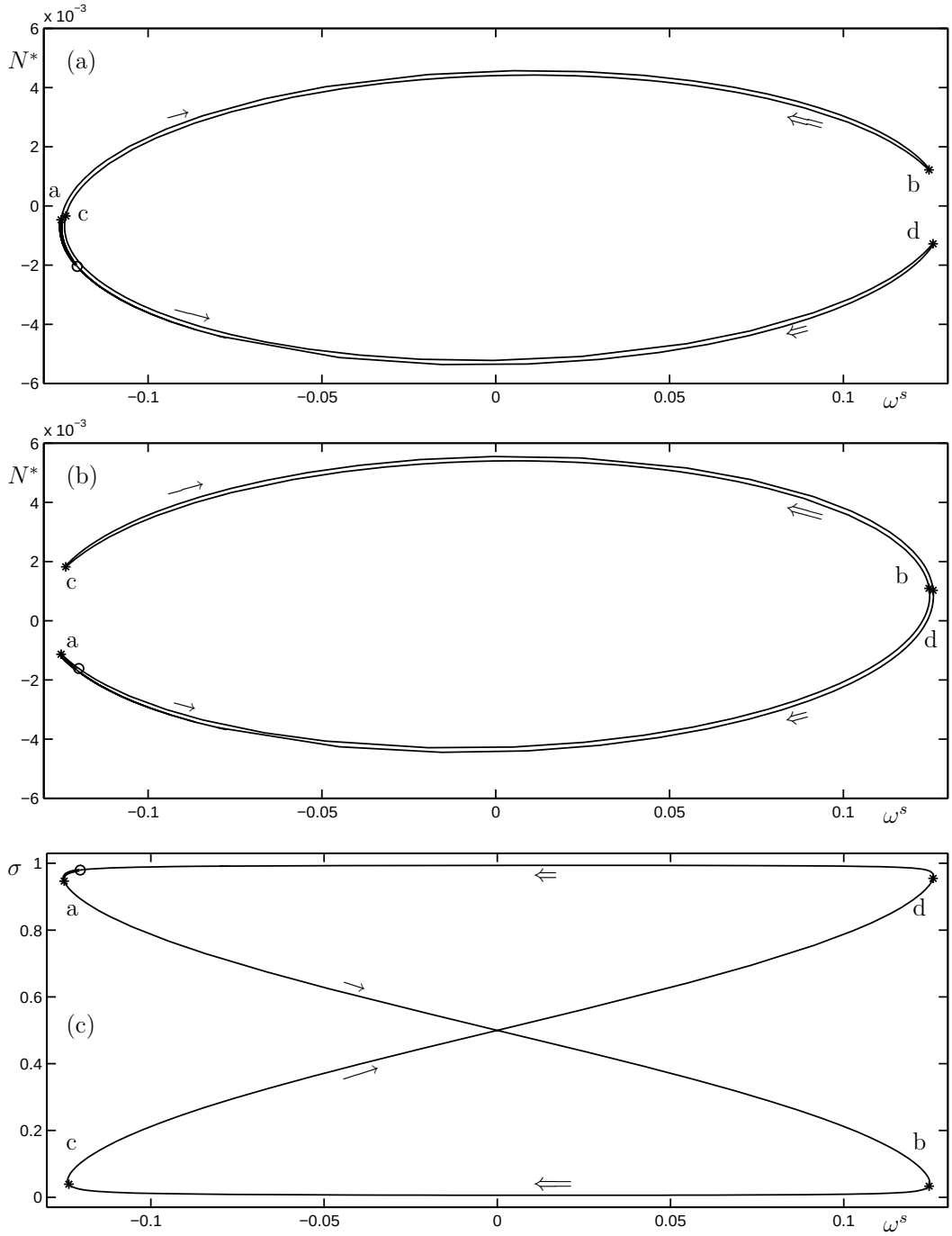

Figure 2. Horseshoes of the blue laser's CLMs (a) and of the red laser's CLMs (b) for $\Delta = 2.5 \times 10^{-3}$ in the (ω^s, N^*)-plane, where $N^* = N - 0.19\omega^s$. Panel (c) shows the phase shift σ in multiples of π as a function of ω^s. The arrows define a direction of movement along the closed curve in the (ω^s, σ)-plane. Different arrows indicate different parts of the curve of CLMs: ($\rightarrow$) decreasing variable-phase CLMs, ($\Longleftarrow$) constant in-phase CLMs, ($\longrightarrow$) increasing variable-phase CLMs, and ($\Leftarrow$) constant anti-phase CLMs. The letters 'a,b,c,d' label the four saddle-node bifurcations; the circle ($\circ$) marks the Hopf bifurcation that bounds the stable part of the branch.

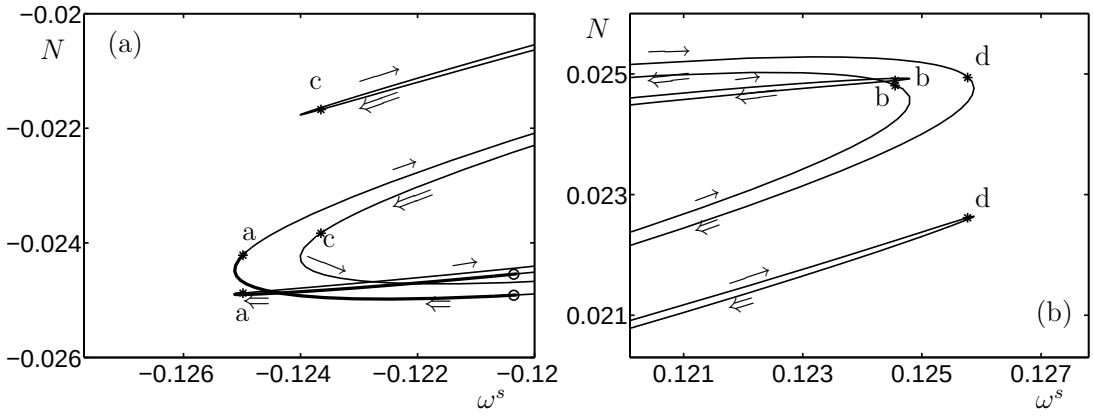

Figure 3. Enlarged view of the (ω^s, N)-plane for $\Delta = 2.5 \times 10^{-3}$ of the low-inversion region (a) and the high-inversion region (b); compare Fig. 1(d) and (f). The letters 'a,b,c,d' label the saddle-node bifurcations; the arrows define the direction of traveling along the branch as in Fig. 2.

corresponds to the lower branch of the lower half of the blue horseshoe and the lower branch of the lower half of the red horseshoe.

From this behavior we can deduce a general rule: branches which can be found on the same half of both laser's horseshoes exhibit almost constant phase. Branches which can be found on different halfs of the horseshoes exhibit variable phase.

We can understand how the red and the blue horseshoes are formed by focusing on the regions around the pitchfork bifurcations for zero detuning in Fig. 1(d) and (e). Figure 3(a) and (b) show an enlarged view of the low-inversion region and the high-inversion region for nonzero detuning. The far edges of the horseshoes can be recognized. This figure should be compared with Fig. 1(d) and (e) for zero detuning. The (ω^s, N)-plane of all these panels show the same range. For zero detuning (Fig. 1(d) and (e)) the constant-phase ellipse and the variable-phase ellipse are only intersecting in two points, the pitchfork bifurcation points. For nonzero detuning the reflection symmetry is destroyed, the pitchfork bifurcations vanish and saddle-node bifurcations and a separated branch of solutions appear instead. This unfolding scheme is well known for pitchfork bifurcations under perturbation of the Z_2-symmetry; see for example [13]. There are two possible unfolding schemes: depending on the sign of the perturbation a separate branch of solutions can be formed above or below the saddle-node bifurcation.

In our system both unfolding schemes exist; the perturbation Δ is negative for laser 1, while it is positive for laser 2. The unfolding processes lead to two types of connections in our system. Consider again Fig. 1(d). Type one connects the upper branch of the variable-phase CLMs and a branch of in-phase or anti-phase CLMs directly underneath. Type two connects the upper branch of the variable-phase CLMs and the lowest branch of in-phase or anti-phase CLMs. These types of connections can be recognized in Fig. 3(a) and (b). Around saddle-node bifurcation 'a' the blue laser performs connection type two and the red laser performs connection type one. Around saddle-node bifurcation 'd' the blue laser performs connection type one and the red laser performs connection type two. These local connections globally lead to the horseshoes already discussed in the previous paragraph.

5. VARIABLE DETUNING

So far we investigated the CLMs for nonzero but fixed detuning and variable C_p. Now we fix the value of C_p in such a way that we are at some point in the stable region of the in-phase CLMs of Fig. 1(c) and take the detuning parameter Δ as variable. In Fig. 4 the inversions N_1 and N_2 are plotted as a function of Δ. A symmetrical figure can be seen. For zero detuning there is always an intersection point between the branch of the red laser and the branch of the blue laser. The remaining four different values of inversion for zero detuning can be recognized as certain points on the upper half and the lower half of constant-phase and variable-phase ellipse of Fig. 1(d). In

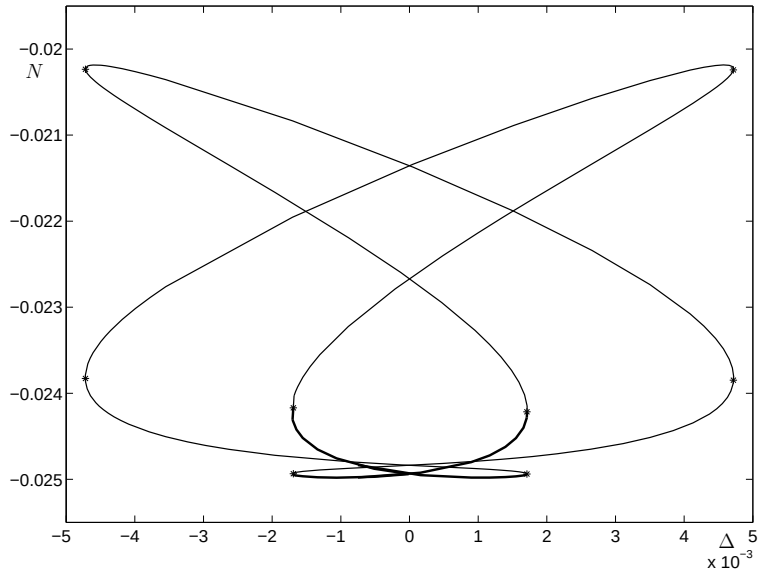

Figure 4. The CLMs in the (Δ, N)-plane for the fixed value of $C_p = 2.9\pi$, and Δ as a free parameter. Stars $(*)$ are saddle-node bifurcations; boldfaced parts of the branch are stable and thin parts are unstable.

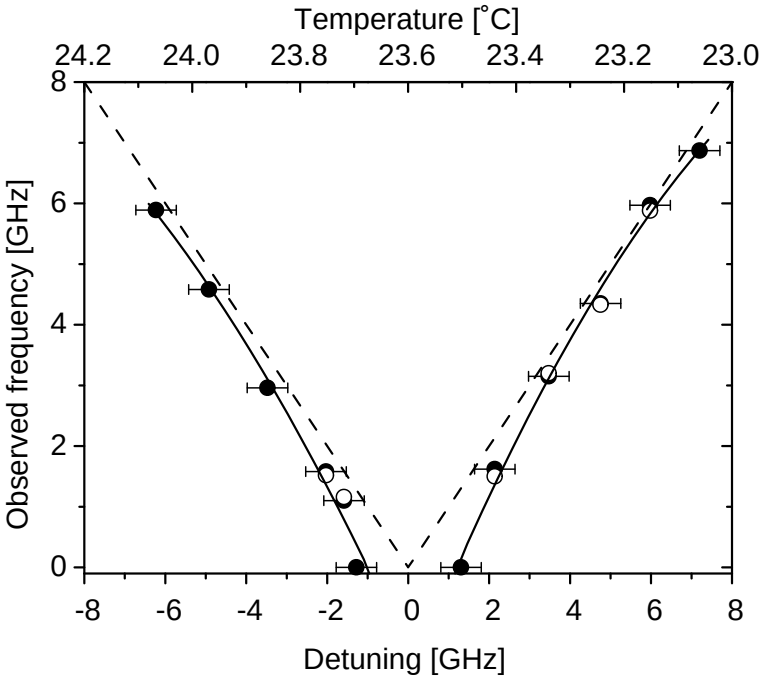

Figure 5. Experimentally observed detuning scenario. The observed frequency of the intensity oscillations is plotted as a function of the detuning. The axis at the top shows the temperature of the heat sink; the dashed line indicates the position of the detuning frequency. Filled circles correspond to laser 1 and open circles to laser 2; the solid curve is an interpolation. A locking region around zero detuning is found. The frequency of the intensity oscillations approach the detuning frequency for large values of detuning.

Fig. 4 bold parts of the branch indicate the existence of stable CLMs. This means that there is a locking region where both lasers have the same frequency. For this particular value of C_p the locking region loses stability via saddle-node bifurcations ($*$). (For other values of C_p the locking region may lose stability via Hopf bifurcations.) Two further saddle-node bifurcation are found. They take place on an already unstable part of the branch.

For large values of detuning well away from the locking region, one finds mixed-mode oscillations. Moving towards the locking region these oscillations may become unstable by undergoing further bifurcations before the locking region is reached. Nevertheless, the frequency of the mixed-mode oscillation may still be dominant. For our parameter values, we found a chaotic attractor just outside the locking region. The saddle-node bifurcation at the boundary of the locking region appears to take place on this chaotic attractor, which is also referred to as an intermittent bifurcation.

In Fig. 5 experimental results from [7] are presented. In this particular setup the coupling time is 0.2 ns, an estimation of the coupling strength gives an upper limit of 8.0×10^9 s^{-1} and both lasers are operated 2.7 times above the threshold. Detuning is achieved by small temperature changes in one laser. The frequency of the dominant peak in the Rf-spectra of the observed intensity oscillations is plotted as a function of the detuning. In the center around zero detuning there is no dominant peak in the Rf-spectra of both lasers, meaning that they have constant intensity. This proves experimentally the existence of the locking region. Outside the locking region the Rf-spectra of both lasers exhibit a distinct peak, due to oscillation in the intensity. At the edges to the locking region the peaks are broadened and the frequency almost goes to zero. For large values of detuning the frequency of the intensity oscillations approaches the detuning frequency. The experimentally broadened peaks in the Rf-spectra at the boundary of the locking region may be an indication of chaotic dynamics. This shows that experiment and theory are in qualitative agreement; see also [8] for more experimental results.

6. SUMMARY AND OUTLOOK

In this contribution we presented a geometrical picture of the CLM structure of two mutually coupled semiconductor lasers. For zero detuning one finds three types of CLMs: in-phase CLMs, anti-phase CLMs, and variable-phase CLMs. The variable-phase CLMs have their origin in pitchfork bifurcations due to a Z_2-symmetry of the system for zero detuning. For nonzero detuning one observes an unfolding of the pitchfork bifurcations into saddle-node bifurcations and separate branches of solutions. This local unfolding has a crucial influence on the global structure of the CLMs, which now form one closed curve in the shape of a horseshoe in (ω^s, N)-plane.

For variable detuning we showed qualitative agreement between theory and experiment. A stable locking region is found around zero detuning, in qualitative agreement with experimental measurements. A detailed and quantative comparison of theory and experiment is beyond the scope of this contribution and will be the subject of future work.

The CLM structure provides the backbone for further studies of the dynamics. The next step will be the study of Hopf bifurcations and their bifurcating periodic orbits. How these orbits undergo further bifurcations to more complicated dynamics will be discussed elsewhere.

REFERENCES

1. J. Mulet, C. Mirasso, T. Heil, and I. Fischer, "Synchronization of two distant mutually coupled semiconductor lasers," *J. Opt. B: Quantum Semiclass. Opt.* **6**, pp. 97–105, 2004.
2. J. Mulet, C. Masoller, and C. R. Mirasso, "Modeling bidirectional single-mode semiconductor lasers," *Phys. Rev. A* **65**, p. 063815, 2002.
3. T. Heil, I. Fischer, and W. Elsäßer, "Chaos synchronization and spontaneous symmetry-breaking in symmetrically delay-coupled semiconductor lasers," *Phys. Rev. Lett.* **86**, pp. 795–798, 2001.
4. S. Yanchuck, K. R. Schneider, and L. Recke, "Dynamics of two mutually coupled semoiconductor lasers: instantaneous coupling limit," *Weierstraß-Institut für Angewandte Analysis und Stochastic* , p. Preprint No. 879, Berlin, 2003.
5. J. Javaloyes, P. Mandel, and D. Pieroux, "Dynamical properties of lasers coupled face to face," *Phys. Rev. E* **67**, p. 036201, 2003.

6. R. Vicente, J. Mulet, M. Sciamanna, and C. Mirasso, "Simple interpretation of the dynamics of mutually coupled semiconductor lasers," *Proc. SPIE Photonics West 2004*, to appear, 2004.
7. H. Erzgräber, *Coupling Phenomena, Instabilities and Synchronisation of Two Mutually Coupled Semiconductor Lasers with Sub-Nanosecond Coupling Time, Diploma Thesis*, Institut für Angewandte Physik, Technische Universität Darmstadt, Darmstadt, Germany, 2002.
8. E. Wille, M. Peil, I. Fischer, and W. Elsäßer, "Dynamical properties of mutually delay-coupled semiconductor laser in the short coupling regime," *Proc. SPIE Photonics Europe 2004*, to appear, 2004.
9. K. Engelborgs, T. Luzyanina, and G. Samaey, *DDE-BIFTOOL v. 2.00 user manual: a Matlab package for bifurcation analysis of delay differential equations. Technical report TW-330.*, Department of Computer Science, K.U. Leuven, Leuven, Belgium, 2001.
10. R. Lang and K. Kobayashi, "External optical feedback on semiconductor injection laser properties," *IEEE Journal of Quantum Electronics* **QE-16**, pp. 347–355, 1980.
11. B. Krauskopf, G. H. M. V. Tartwijk, and G. R. Gray, "Symmetry properties of lasers subject to optical feedback," *Opt. Commun.* **177**, pp. 347–353, 2000.
12. T. Heil, I. Fischer, B. Krauskopf, K. Green, and A. Gavrielides, "Delay dynamics of semiconductor lasers with short external cavities: Bifurcation scenarios and mechanisms," *Phys. Rev. E* **67**, p. 066214, 2003.
13. S. H. Strogatz, *Nonlinear Dynamics and Chaos*, Perseus Books, Reading, Massachusetts, 1994.